International Society for Rock Mechanics and Rock Engineering
Norwegian Group for Rock Mechanics

ISRM International Symposium
Eurock 2025 – Expanding the Underground Space
Trondheim, Norway, 16-20 June
ISBN 978-82-8208-079-8

Simulation of Slope Movements at Åknes using 2D Distinct Element Modeling

C. Cancino & L. Lorig
ITASCA, Minneapolis, USA
ccancino@oneitasca.com

Abstract

The Åknes rock slope is a large, slow-moving mass of foliated gneiss in western Norway. This slope is considered to have a high-risk failure potential, with an area of 0.56 km^2 and an estimated volume of more than 50 million m^3 (Pless et al., 2021) and parts that are moving 2–8 cm per year. If a rockslide were to fall suddenly into the fjord below, large, destructive tsunami waves would result. Because of this risk, several national and international groups participated in a major site investigation and monitoring program consisting of extensometers, crackmeters, tiltmeters, single lasers, GPS, total station, ground-based radar, geophones, climate station, and borehole inclinometers and piezometers. The resulting data indicates continuous movement all year, but with significant seasonal differences. The rate of movement can increase up to 1 mm per day, or ten times the annual mean, during times of snowmelt and heavy precipitation.

General drainage concepts have been discussed for well over a decade, but without the benefit of rigorous quantitative support. This paper summarizes a two-dimensional numerical assessment aimed at understanding key elements of the landslide mechanism and evaluating drainage mitigation. The calibrated model suggested that eliminating 50% of the infiltrating runoff in the upper part of the slope would reduce rainfall-induced displacements by approximately 80%.

Keywords

Slope Stability, Numerical Modeling, Åknes Landslide, Distinct Element Modeling, Drainage.

1 Introduction

The Norwegian Directorate for Civil Protection has named the Åknes rockslide as one of the most consequential potential events in Norway, with high risks for harm to citizens and to the economy (Pless et al., 2021). Per Åknernes, who lived on a farm below the slope, identified the Åknes rock slope in the 1960s, and many studies have been conducted in the last 40 years to aid in understanding the rockslide risks. The Norwegian Water Resources and Energy Directorate (NVE) has been tasked with continuing the investigation of methods to clarify the potential dangers and reduce the risk of a failure at the slope.

The Åknes Drainage Project aimed to study geological and hydrogeological conditions as well as the potential efficacy of drainage in mitigating risk. Large-scale drainage of landslides has been shown to aid in the stability of rock slope hazards and significantly reduce velocities (Eberhardt et al., 2007; Lin et al., 2020). Instances of increased precipitation and groundwater levels at the Åknes slope have shown measurable increases in displacement velocities. Therefore, as part of this project, a 2D Distinct Element Modeling assessment was carried out to better understand the rockslide mechanism and to assess if a different drainage scheme will effectively reduce risks associated with a sudden failure of the slow-moving rockslide.

2 Background

2.1 Literature Review

Grimstad (1989) carried out one of the first stability analyses at Åknes. Based on shallow boreholes, Grimstad estimated a potential sliding plane at a depth of 15-45 m with an average of 20 m. This sliding plane, currently known as the upper sliding plane, was later highlighted by studies using deeper boreholes. Sensitivity analyses carried out by Grimstad (1989) for differing depths of the sliding plane suggested that the factor of safety decreases with depth of the sliding plane, and that increasing pore pressure to 10 m above the sliding plane will reduce the factor of safety below 1.0.

The Norwegian Geotechnical Institute (NGI, 1996) used many of the same input parameters in their numerical modeling that Grimstad did in his computations. The numerical modeling mainly confirmed Grimstad's findings, with an unstable zone between 550 and 900 meters above sea level, with the western flank unstable even after extended dry periods and the eastern flank stable when dry.

Later, Kveldsvik et al. (2009) used both discontinuous deformation analysis (*DDA*) and the Universal Distinct Element Code (*UDEC*) in their numerical models. According to Kveldsvik et al, increases in the groundwater table are less critical for a very deep slope instability (200 m depth) than for a shallower instability (70 m depth). They also suggested that a shallow failure would reduce the stability of the slope at greater depths.

In another study, Kveldsvik et al. (2009) used dynamic numerical modeling to evaluate the Åknes slope stability during earthquakes. According to their analysis, a 1000-year earthquake is expected to trigger an instability under current groundwater conditions, but if the slope is drained for this modeled seismic event, the slope would be stable.

Grøneng et al. (2010) carried out a numerical assessment of the long-term stability of the slope using the Burger-Creep Viscoplastic (*CVISC*) material model in *FLAC3D*, reporting a stable slope when assuming good surface condition at the sliding surface. However, due to gradual reduction in the shear strength parameters over time, lower parts of the slope became unstable and increased surface displacements were observed in the same time span. Modeling shows this behavior occurs when fair surface conditions are assumed with a composite sliding layer with only 1% of intact rock bridges, 35% gouge and 64% unfilled joints and a fractured rock mass corresponding to a Geologic Strength index (GSI) of 37.

Langeland and Blikra (2014) simulated the stability of the upper area of the Åknes slope with different groundwater levels and strengths for the sliding zone. According to the model, a 4 m rise in water level has a significant impact on the velocity rates, while a 6 m rise has a critical effect on the stability. Even at normal groundwater levels, a 10% reduction in shear strength of the shear zone resulted in total collapse of the slope. According to Langeland and Blikra (2014), a decrease of the shear zone strength can have a larger effect on the stability of the slope than groundwater levels.

2.2 Geological Model

The Åknes slope, facing southward, has an average dip angle of 30–35° from the fjord (sea level) to an elevation of 1000 m over a distance of 1400 m. Ganerød et al. (2008) developed a geological model after extensive fieldwork. Using field observations and geophysical data, the rockslide was divided into four sub-domains (Figure 1) experiencing extension in the upper part and compression in the lower part. Ganerød et al. (2008) suggest that there is an undulating basal sliding surface with subordinate sliding surfaces that crop out at least two main levels, one in the middle of the slope and one closer to the toe.

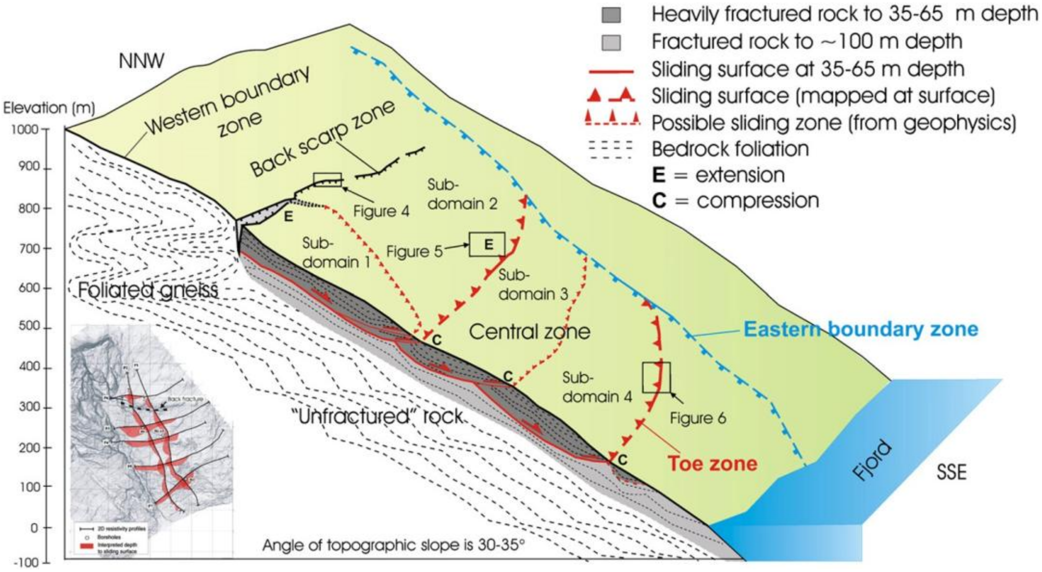

Fig. 1 Geological model of the Åknes rockslide (Ganerød et al., 2008).

The folded foliation, generally dipping at 30-40° S-SSE (towards the fjord and subparallel to the slope surface), controls the development of the basal sliding surface with its subordinate low angle surfaces. In addition to the foliation parallel fracture set (S-SSE), two near vertical sets have been mapped striking N-S and E-W.

Jaboyedoff et al. (2011) improved the understanding of the geological model and suggested the presence of a set of E-W striking folds perpendicular to the direction of the main movement of the rock mass. According to the investigation, the majority of the sliding surface develops along the foliation, although it is not restricted to single layers in the foliation, but rather steps down along subvertical cracks that have developed parallel to the folds.

Langeland and Blikra (2014) suggested a new model for the western flank area based on data from borehole instrumentation. Borehole movement measurements indicate that there are two sliding surfaces in this location, with the deeper one being predominant. The primary sliding surface daylights in the NNW-SSE trending valley known as Åknesrenna, which constitutes the instability's western limit. Based on geophysics and borehole cores, an even deeper sliding surface is hypothesized, and Langeland and Blikra (2014) also assumed some steps in the sliding surfaces following the E-W subvertical joint set, validating previous interpretations.

2.3 Displacement Data

Five extensometers are positioned along the middle portion of the backscarp, and Global Navigation Satellite Systems (GNSS) receivers, two lasers with reflectors, and a total station with thirty prisms are spread out over the monitored region on the Åknes rock slope (Figure 2). NORSAR has installed a broadband seismometer, a ground network of five geophones, and an eight-geophone borehole string in the vicinity. At 900 masl, there is also a weather station. In addition to the on-site instrumentation, the Åknes slope has a total of twelve boreholes, seven of which are equipped with inclinometers and piezometers, and the rockslide has been tracked remotely since 2005 using periodic ground-based Interferometric Synthetic Aperture Radar (InSAR) readings and satellite-based INSAR.

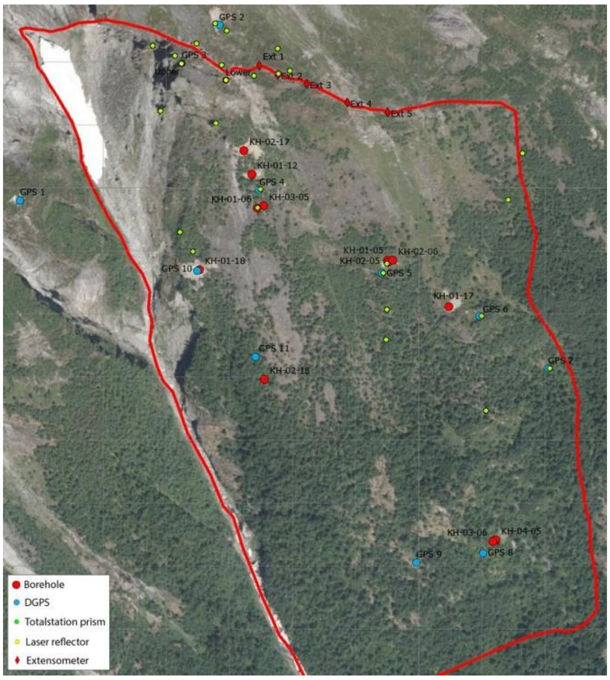

Fig. 2 Overview of boreholes and instrumentation at the Åknes rockslide (Pless et al., 2021).

3 Numerical Assessment

3.1 Approach

The fundamental considerations regarding Åknes are the following:

- Deformation rates increase during times of enhanced precipitation.
- Measured displacement rates are very slow outside of times of enhanced precipitation.
- Water is believed to play a fundamental role in slope behavior.
- The total amount of deformation required to “fail” the slope is unknown.
- If deformation can be slowed or stopped, the likelihood of slope failure is decreased.

Simulating time-dependent creep in numerical models is often an exercise in calibrating non-physical parameters that are not necessarily related to the presence of water. Therefore, it was decided not to pursue creep modeling at this time, but rather focus on physical parameters that are known to impact slope behavior.

The chosen approach is to use the enhanced precipitation event around autumn 2018 to calibrate the friction of discontinuities in the rock mass to approximately reproduce measured surface displacements during that time. The calibration is aided by consideration of historical subsurface deformation patterns. The base case water pressures (i.e., typical water pressures outside times with enhanced precipitation) and calibrated frictions will then be used to assess if proposed mitigation measures will result in a reduction of base case water pressures. The effectiveness of mitigation measures is determined by comparing rainfall-induced displacements for the unmitigated and mitigated cases.

The main advantage of this approach, as opposed to the traditional factor of safety approach used in previous numerical assessments, is that it utilizes updated displacement data to back-analyze the overall performance of the rock mass in order to build a model that would be able to provide a forward prediction of the impacts of drainage on the displacements of the rock mass.

Considering the 2020 topography mapped by drone (Figure 3A), two-dimensional analyses along the dashed red line shown in Figure 3B are reported here. This profile was selected to be representative of the moving area and is also near installed instrumentation. Other researchers (Grøneng, 2010; Oppitokofer et al., 2011) have also used similar section lines to illustrate key elements of the slope. Measurements show that the slope is not moving directly down the line of analysis, but more towards the valley (also called the western boundary zone) to the west of the line of analysis, particularly in the upper part of the slope.

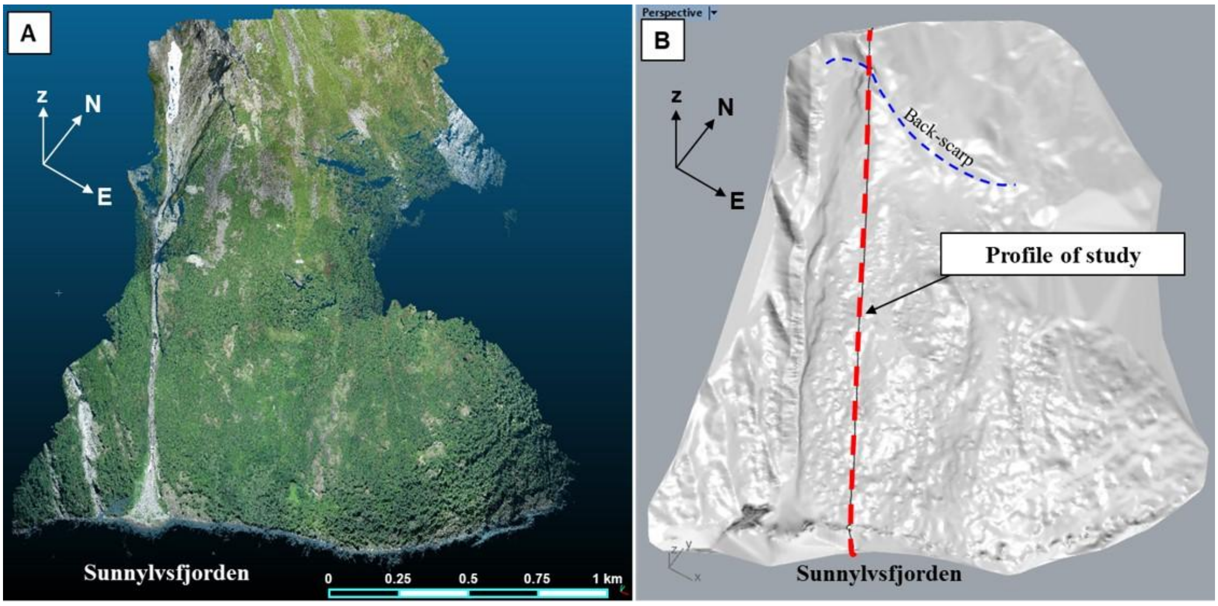

Fig. 3 (A) 2020 topography mapped by drone. (B) Profile of study based on 2020 topography.

3.2 Assumptions

The fundamental assumption inherent in this work is that reducing deformation rates will reduce landslide risk. The following additional assumptions apply:

- Background (steady-state or creep) movements are not part of this current study. The focus is on movements associated with spring snowmelt and heavy precipitation events. Efforts to reduce seasonal movements are expected to also impact background movements positively.
- No stochastic modeling has been performed at this time. All analyses are deterministic.
- No fully dynamic (time domain) analyses are part of this study.
- Only one-way hydromechanical coupling is considered in this work. One-way hydromechanical coupling involves specifying spatial distribution of water pressures within the slope.

3.3 Calibration Background

As mentioned previously, there is a great deal of site information that has been collected over recent years. This section highlights some of the information used in developing the numerical model.

3.3.1 Surface Deformation Patterns

The overall surface deformation patterns are inferred from InSAR monitoring, surface markers (prisms), etc. It is well understood that movement rates increase during times of increased precipitation.

Autumn 2018 has been highlighted as a season of particularly heavy rainfall (from 15 September to 30 October 2018). The movement data for this period is shown in Figure 4 and Table 1, which shows that the average displacement rate for the autumn 2018 event was 0.19 mm/day. Before and after autumn 2018, rates were nearly half of that. Figure 5 shows only the deformations related to the autumn 2018 event (47 days). Various parts of the slope moved in the vicinity of the analysis section and that the upper part of the slope moved more than the lower part of the slope. This pattern is consistent with the overall history of the slope. The movement shown in Figure 5B is used for calibration of the numerical model.

September and October precipitation [mm]									
2012	2013	2014	2015	2016	2017	2018	2019	2020	Average
343.8	159.1	231.6	123.4	158.3	274.7	521.8	363.6	244.5	269

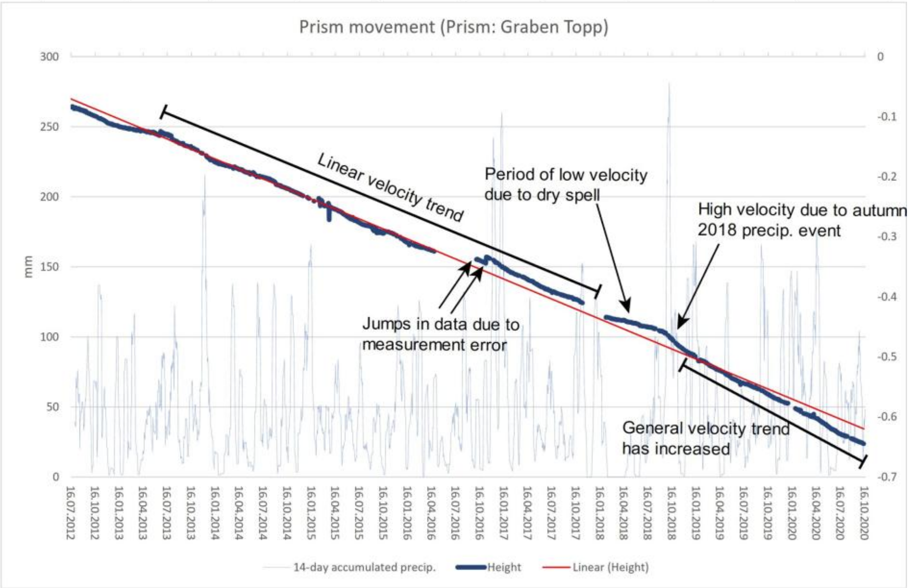

Fig. 4 Surface marker velocities before, during, and after the autumn 2018 rainfall event.

Table 1 Marker velocities before, during, and after the autumn 2018 rainfall event.

Instrument	2016-2018 velocity [mm/day]	Autumn 2018 event velocity [mm/day]	2018-2020 velocity [mm/day]
Berg 2	0.054	0.189	0.053
Graben GPS	0.159	0.266	0.203
Graben nedre	0.213	0.434	0.271
Graben top	0.217	0.445	0.270
Kant	0.146	0.235	0.176
Knaus	0.005	0.082	0.006
Kul GPS	0.036	0.104	0.039
Nedre laser prisme	0.006	0.023	0.002
Nedre laser reflector	0.157	0.264	0.196
Ny gps	0.141	0.327	0.171
Ny 2010	0.040	0.054	0.034
Ormebolet GPS	0.060	0.084	0.065
PGPS6	0.062	0.168	0.061
Prisme 3	0.007	0.104	0.005
Renne 10	0.179	0.306	0.214
Skog	0.004	0.022	0.011
Stein 2	0.005	0.028	0.008
Øvre borrplass	0.108	0.289	0.147
Average	**0.089**	**0.190**	**0.107**

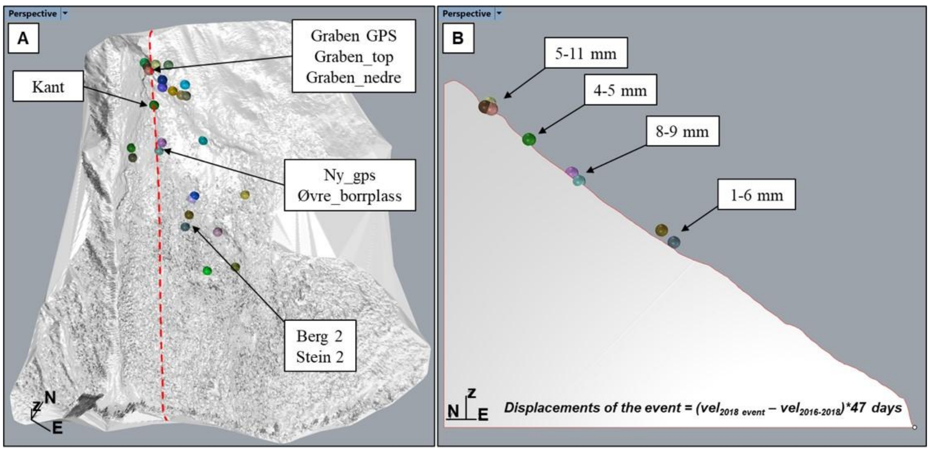

Fig. 5 (A) Surface instrumentation location at Åknes rockslide. (B) Surface displacement magnitude along section of analysis during the autumn 2018 event.

3.3.2 Subsurface Deformation Patterns

Subsurface deformation patterns are measured in inclinometers at a few locations in the slope. As an example, Figure 6 shows the pattern along the borehole KH-02-17. The borehole data suggest discontinuous deformation at depths of about 30 m and 70 m below the collar (i.e., ground surface). Other instruments show a larger offset at a depth of 70 m compared to the offset at 30 m depth. These two depths correspond to weak zones identified as "fracture corridors". Two fracture corridors have been introduced into the numerical model at vertical distances around 30 m and 70 m below the ground surface by assuming a lower friction angle for the slope parallel structures at these depths compared to elsewhere.

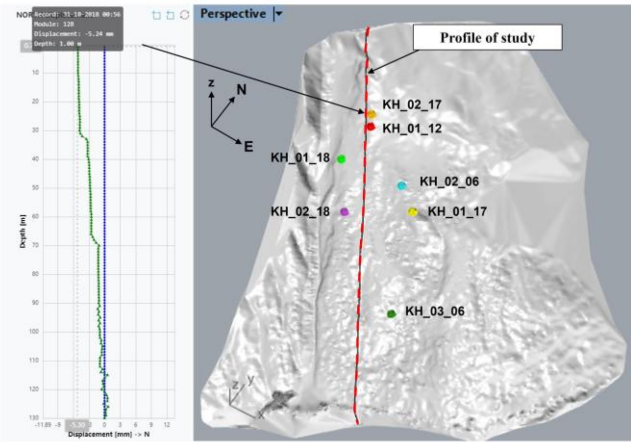

Fig. 6 Subsurface deformation pattern at borehole KH-02-17.

3.4 2D Distinct Element Model

The Universal Distinct Element Code, *UDEC* (Itasca, 2019), was chosen for this study because of its ability to explicitly include many discontinuities. Discontinuities separate the rock slope into individual blocks that may slide and separate. Block behavior may be assumed to be rigid, elastic, or elastic-plastic. In this case the blocks were assumed to behave elastically, i.e., they cannot fail internally. As discussed later, this is a limitation in the current model; however, it is considered to be a reasonable assumption given the high strength of intact rock under a low stress condition. The numerical model is based on a conceptual model similar to the one developed by Oppikofer et al. (2011) (Figure 7). The key feature of this model is the decreasing dip of the potential sliding discontinuities in going from the slope crest to the slope toe as presented in the bottom of Figure 7. Note that the minimum dip assumed in the *UDEC* model is 30° (instead of 25°) based on the geological model developed by Ganerød et al. (2008). In addition to the sliding surfaces from Figure 7, the *UDEC* model includes vertical discontinuities that likely are responsible for the steps seen in the sliding surfaces in Figure 8. Three distinct layers of rock block sizes are also included, similar to that shown in Figure 9. The resultant *UDEC* model is shown in Figure 10. The uppermost layer corresponds to a highly fractured region with seismic velocity less than 2000 m/s. The bottom of the second layer is located 100 m below the surface and corresponds roughly to the lower limit of more intensely fractured rock with higher permeability. It is important to note that the *UDEC* model is necessarily an idealized representation of reality, not a faithful reproduction of reality.

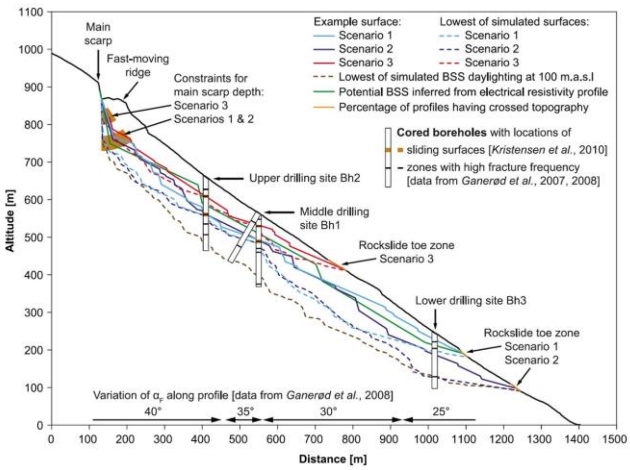

Fig. 7 Conceptual mechanical model showing potential deformation surfaces (modified from Oppikofer et al., 2011).

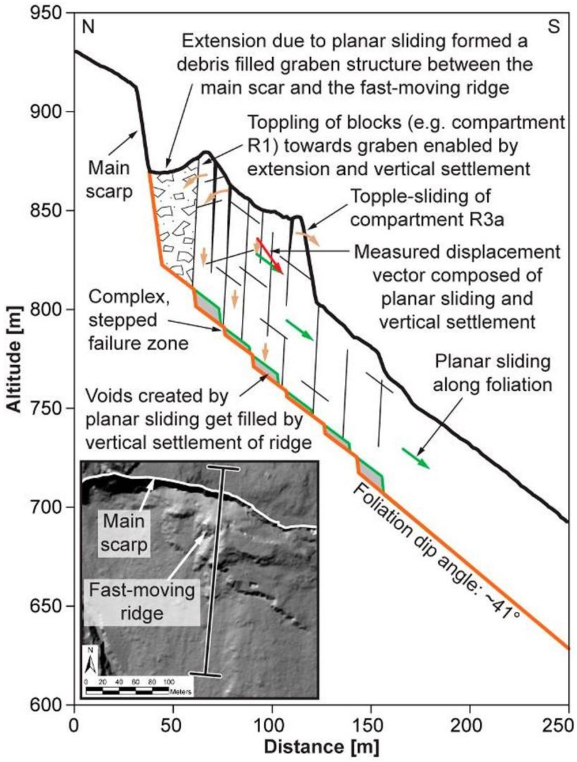

Fig. 8 Near-vertical joints forming a complex stepped failure surface (from Oppikofer et al., 2009).

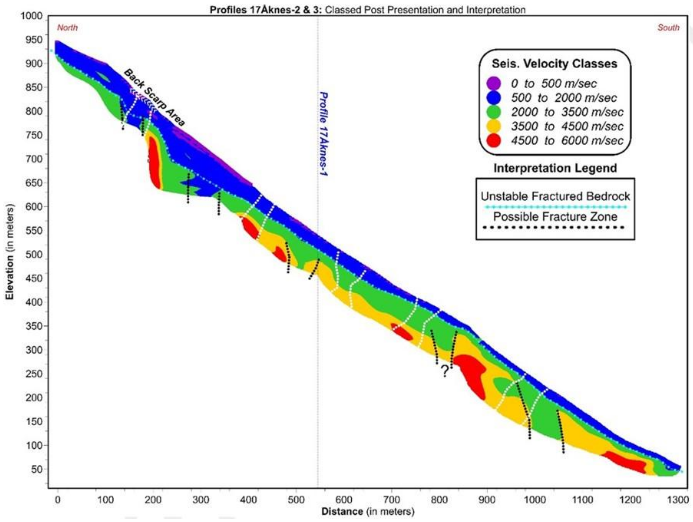

Fig. 9 Rock mass domain model based on seismic refraction data (Tassis, 2019).

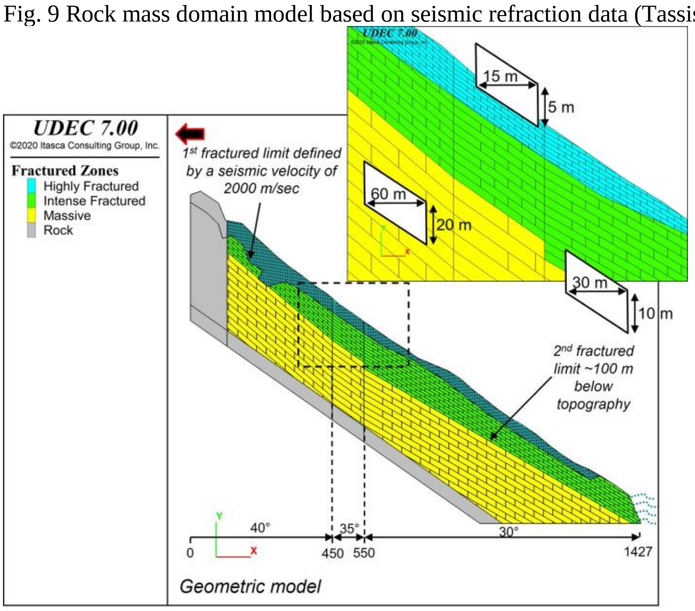

Fig. 10 *UDEC* model showing three layers of fracturing.

3.4.1 Discontinuity Strengths

Trials were used to determine discontinuity strengths in an attempt to match both the surface displacement pattern caused by heavy rain in autumn 2018 and the general pattern of subsurface displacement. There is no cohesive or tensile strength assumed in any discontinuity. The strengths of the slope-parallel fractures in the model are as follows:

- 50° friction angle in the highly fractured rock mass layer (upper layer);
- 50° friction angle in the intense fractured rock mass layer (middle layer); and
- 60° friction angle in the massive rock mass layer (lower layer).

A 50° friction angle was estimated for all vertical joints. For the fracture corridors, various assumptions have been studied, but only one is reported here, which assumes a 38° friction angle in both fracture corridors (30 m and 70 m below surface). No significant difference was observed when different friction angles were applied to the fracture corridors assuming that the lower fracture corridor could be weaker than the upper one.

While it may seem that the discontinuities have relatively high friction angles, it is important to note that they have zero cohesion and normal stresses are relatively low. Similar results might be produced with lower assumed friction and a small amount of cohesion.

3.4.2 Water Pressures

Sena and Braathen (2021) developed three-dimensional hydrogeological models that are the base for all water pressures included as water tables in this study. Below the water table, hydrostatic water pressures are assumed. Four different water tables are assumed:

- Base case: The current background water level is represented by this case.
- Base case with autumn 2018 event: This scenario depicts the rise in water level as a result of the autumn 2018 event.
- Base case with 50% cutoff of recharge of the upper slope: This is the future mitigated water level.
- Base case with 50% cutoff and intense rainfall: This is the future mitigated water level owing to heavy rainfall comparable to that seen in autumn 2018.

The four assumed water levels are shown in Figure 11. Note that a vertical back scarp 80 m high was assumed in the model.

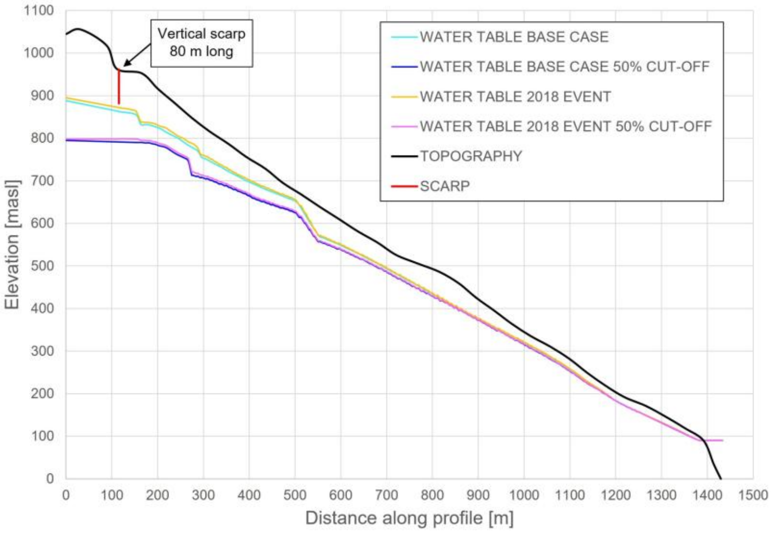

Fig. 11 Water tables assumed in the analyses.

4 Results

This section presents results comparing modelled and measured displacements due to the autumn 2018 rainfall. These results demonstrate that the model is capable of reproducing the measured displacements using reasonable assumptions for discontinuity strength. This section also presents results for a similar future rainfall event assuming that mitigation measures are introduced to reduce recharge in the upper slope by 50%.

4.1 Calibration Results

Figure 12 presents displacement contours resulting from introduction of the autumn 2018 rainfall event into the *UDEC* model. A reasonable agreement between measured and modelled surface displacements is demonstrated by looking at the measured displacement shown in the inset. Figure 13 shows the displacements with depth at the location of KH-02-17. A displacement discontinuity is clear at a depth of 70 m, suggesting slip along the deeper fracture corridor. Slip at the upper fracture corridor is not evident. It should be noted that the upper fracture corridor is located above the assumed base case water table for most of its length.

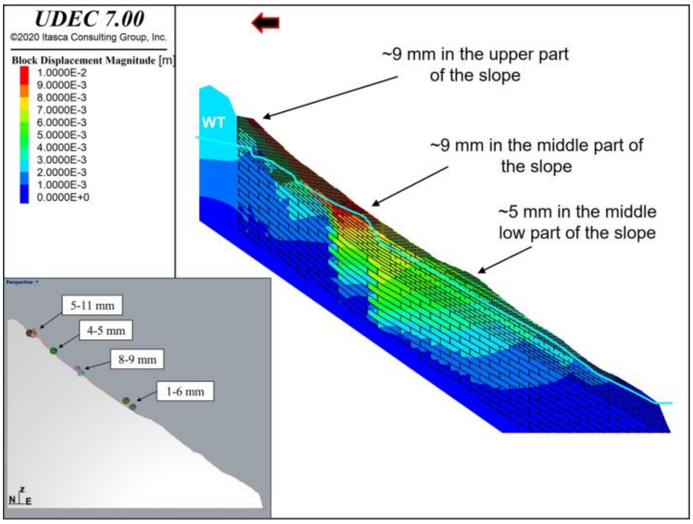

Fig. 12 Displacement contours (m) resulting from introduction of the autumn 2018 rainfall event into the *UDEC* model. Measured displacements from the autumn 2018 event are shown in the inset for comparison.

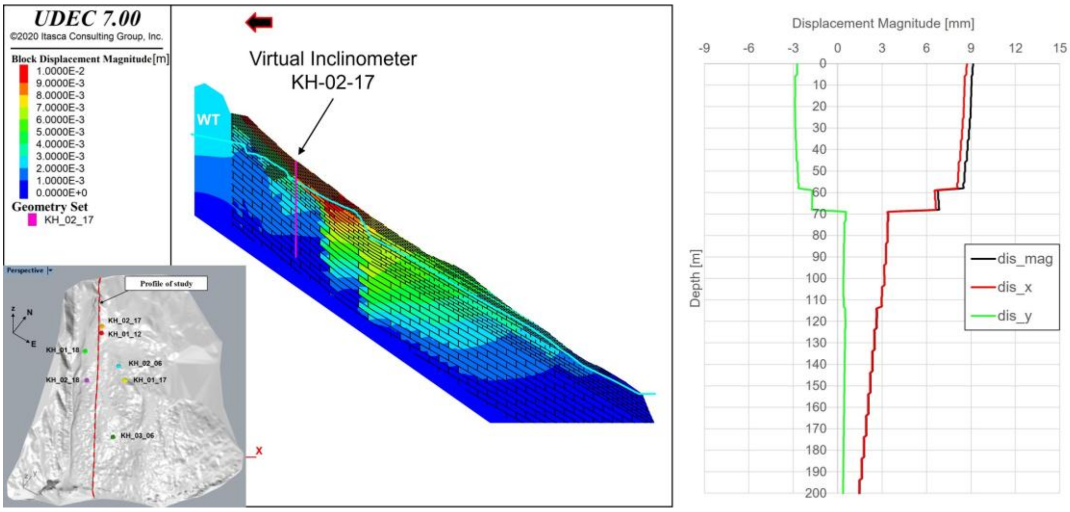

Fig. 13 Displacement contours (m) within the model and at the virtual extensometer KH-02-17 resulting from introduction of the autumn 2018 rainfall event.

It is important to note that although a reasonably good calibration has been achieved, the parameters used are not unique. It is possible that other parameter sets could produce similar or even closer agreement.

4.2 Predictive Results for Mitigated Case

The results shown in this sub-section relate to the case where only 50% of future runoff is allowed to enter the upper part of the slope. Figure 14 shows the predicted displacements for a future rainfall event for the mitigation case. Comparing Figure 12 (unmitigated case) with Figure 14 (mitigated case) shows that future displacements would be reduced by about 80% for the calibrated case. This observation also correlates well with measured slope movements in periods with low and high precipitation, and with international experience, where drainage measures have been successfully implemented (Pless et al., 2021).

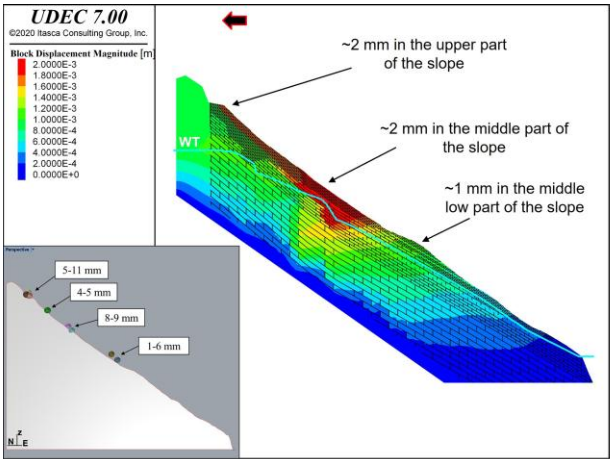

Fig. 14 Displacement contours (m) resulting from introduction of the autumn 2018 rainfall event, but with mitigation resulting in 50% less recharge to the upper slope. Measured displacements from the autumn 2018 event are shown in the inset for comparison.

5 Discussion

This paper has shown that reasonable assumptions and parameters can be used in a two-dimensional numerical model to explain displacements resulting from increased rainfall events such as occurred in autumn of 2018. It should be noted that the model is an idealization, not a precise reproduction, of reality. Models exhibit important mechanisms and behaviors without necessarily understanding all the details of the real problem. Idealized models are made because the real world is often too complex to understand. If complex models are made, they also may be too complex to understand. Authors claim that this model is calibrated because it is capable of reproducing measured and observed slope behavior, but they do not claim that this model is uniquely correct.

Furthermore, the numerical analysis agrees that most of the sliding surface develops along the foliation, but that it is not limited to single layers in the foliation but rather steps down through subvertical cracks with the back-scarp limiting the movement in the upper area.

According to this model, removing half of the infiltrating runoff in the upper part of the slope reduces rainfall-induced displacements by around 80%. The background time-dependent creep behavior of the slope at normal times, i.e., when there is no excessive precipitation, was not studied in this work. However, similar or even greater reductions in background displacements are expected if the mitigation is implemented.

Finally, considering all the assumptions and limitations of the current model, more detailed future studies are recommended. The modeling can be extended and improved in several ways as discussed below in the perceived order of importance:

- Block Failure: The current model assumes that all blocks are elastic. This assumption may inhibit some failure modes by not allowing potential failures through blocks. Future models should consider ubiquitous joints to simulate gneissic foliation.
- Three-dimensional Analysis: The slope under consideration is three-dimensional. The two-dimensional modeling described here can be extended to three dimensions using the numerical modeling code *3DEC* (Itasca, 2019).
- Probability of Failure Analysis: Probability of Failure is a good measure of the effectiveness of mitigation because it is better understood by most people. Probability of Failure requires an estimate of the range and distribution of each of the friction parameters, which is not currently available.
- Fracture Flow Analysis: Both *UDEC* and *3DEC* can simulate flow in fractures to perform a fully coupled hydromechanical analysis. Simulating fracture flow would enhance the analysis by providing a more realistic simulation of water flow within the rock mass and eliminating the need to map water pressures from an equivalent porous media flow model into the mechanical model.
- Creep Analysis: Observed time-dependence in slopes can be attributed to one or more time-dependent mechanisms like direct (and general) groundwater redistribution due to changed

loading; creep of localized low-permeability materials containing trapped water; intrinsic creep of materials such as salt, potash, etc.; stress corrosion in competent rock; stress corrosion at contacts of a granular medium such as quartz sand or sandstone; weathering; chemical changes (and hence strength changes) due to new exposures, etc.

- Dynamic Analysis: Dynamic analysis can be performed by inputting an acceleration (or velocity) time history from an earthquake record (real or artificial) into the base of the numerical model.

6 Acknowledgments

It is important to note that the study shown here benefitted greatly from frequent interaction with and constructive comments from the following members: Lars Blikra and Gustav Pless (NVE), Tom Stewart (BC Hydro), Corey Froese (BGC Engineering), and Clara Sena and Alvar Braathen (University of Oslo).

References

Eberhardt, E., Bonzanigo, L., and Loew, S. (2007). Long-term investigation of a deep-seated creeping landslide in crystalline rock. Part II. Mitigation measures and numerical modelling of deep drainage at Campo Vallemaggia. Canadian Geotechnical Journal. 44(10): 1181-1199. https://doi.org/10.1139/T07-044

Ganerød, G.V., Grøneng, G., Rønning, J.S., Dalsegg, E., Elvebakk, H., Tønnesen, J.F., Kveldsvik, V., Eiken, T., Blikra, L.H., Braathen, A. (2008). Geological model of the Åknes rockslide, western Norway. Eng Geol 102 (1–2):1–18. https://doi.org/10.1016/ j.enggeo.2008.01.018.

Grimstad, E. (1989). Stabilitetsvurdering omkring Remnane ved Åkernes I Stranda. Trondheim, Norway.

Grøneng, G. (2010). Stability Analyses of the Åknes Rock Slope, Western Norway. Doctoral thesis at the Norwegian University of Science and Technology. ISBN 978-82-471-2015-6.

Itasca Consulting Group Inc. (2019) UDEC (Universal Distinct Element Code), Version 7.0. Minneapolis: Itasca.

Itasca Consulting Group Inc. (2019) 3DEC (3-Dimensional Distinct Element Code), Version 7.0. Minneapolis: Itasca.

Kveldsvik, V., Einstein, H., Nilsen, B. and Blikra, L. (2009). Numerical analysis of the 650,000 m2 Åknes rock slope based on measured displacements and geotechnical data. Rock Mechanics and Rock Engineering, 42(5), 689-728. https://doi.org/10.1007/s00603-008-0005-1

Kveldsvik, V., Kaynia, A., Nadim, F., Bhasin, R., Nilsen, B., and Einstein, H. (2009). Dynamic distinct-element analysis of the 800 m high Åknes rock slope. International Journal of Rock Mechanics and Mining Sciences, 46(4), 686-698. https://doi.org/10.1016/j.ijrmms.2008.10.007

Langeland, H. and Blikra, L. (2014). Utvikling av revidert geologisk model log stabilitetanalyser for øvre deler av ustabil fjellside på Åknes.

Lin, D.-G., Chang, K.-C., Ku, C.-Y., and Chou, J.-C (2020). Three-Dimensional Numerical Investigation on the Efficiency of Subsurface Drainage for Large-Scale Landslides. Applied Sciences 10, 3346. doi:10.3390/app10103346.

Norwegian Geotechnical Institute (1996). Åknes landslide: Numerical simulation of the Åknes landslide using universal distinct element code (UDEC). Trondheim, Norway.

Oppitokofer, T., Jaboyedoff, M., Pedrazzini, A., Derron, M. and Blikra, L. (2011). Detailed DEM analysis of a rockslide scar to characterize the basal sliding surface of active rockslides. Journal of Geophysical Research: Earth Surface, 116(2). https://doi.org/10.1029/2010JF001807.

Oppikofer, T., M. Jaboyedoff, L. H. Blikra, and M. Derron. (2009) "Characterization and monitoring of the Åknes rockslide using terrestrial laser scanning," Nat. Hazards Earth Syst. Sci., 9, 1003–1019, doi:10.5194/nhess-9-1003-2009.

Pless, G., Blikra, L., and Kristensen, L. (2021). Possibility for using drainage as mitigation to increase the stability of the Åknes rock-slope instability, Stranda in western Norway. Norwegian Water Resources and Energy Directorate Rapport nr. 22/2021. ISBN: 978-82-410-2147-3. Oslo.

Sena, C., and Braathen, A. (2021). Åknes rock-slope failure hydrogeology – Final report. (February). University of Oslo. Oslo.

Tassis, G. (2019). Reprocessing of Refraction Seismic data from Åknes, Stranda Municipality, Møre and Romsal County. NGU report 2019.004. Trondheim.